Liquid Crystal Biosensing Platform Based on Whispering Gallery Mode Laser for Aβ42 Detection

Peiyao An[a], Mengxiao Li[a], Shanshan Zhang[a], Di Lian[a], Chuqi Li[a], Chuan Wang[b], Miao Yu[a], Duo Wang[a], Lingyi Kong[c], Jun Ren[b], Yue Li[d], Haiyan Wang[e], Xin Yang[f], Zhenlin Wu[a,]*

[a] School of Optoelectronic Engineering and Instrumentation Science, Dalian University of Technology, Dalian, 116024, China.

[b] School of Bioengineering, Dalian University of Technology, Dalian, 116024, China.

[c] DUT-BSU Joint Institute, Dalian University of Technology, Dalian, 116000, China.

[d] Dalian Women and Children's Medical Group, Dalian, 116033, China.

[e] Dalian International Travel Healthcare Center (Dalian Customs Port Clinic), Dalian, 116007, China.

[f] Department of Electrical and Electronic Engineering, School of Engineering, Cardiff University, Cardiff CF24 3AA, United Kingdom.

* Corresponding author: zhenlinwu@dlut.edu.cn

Abstract: Alzheimer's disease (AD) is an irreversible and progressively worsening neurodegenerative disorder. Amyloid beta (Aβ42) plays a crucial role in the early diagnosis of this disease. However, the concentration of Aβ42 in the blood is extremely low, which poses a challenge for Aβ42 detection. Herein, a liquid crystal (LC) biosensing platform based on whispering gallery mode (WGM) laser was developed for rapid and real-time monitoring of the AD-related biomarker Aβ42. The LC microcavities were functionally modified using cetyltrimethyl ammonium bromide (CTAB) and RNA aptamers. Based on this, the quantitative monitoring mechanism of Aβ42 was analyzed, stemming from the interaction between the negatively charged

RNA aptamer and CTAB, leading to the reorientation of LC molecules. This alters the refractive index distribution within the microcavity, thereby enabling the shift of the WGM spectrum. The dynamic changes of molecular orientation in the LC microcavity were monitored by polarization optical microscopy and spectral analysis. The experimental results showed that the total shifts in the resonance spectrum were directly proportional to the concentration of Aβ42 within the range of 0-1000 pg/mL. The sensitivity of the sensor is 0.003 nm/pg/mL. The experiment further confirmed the practicability of this sensor in the mouse serum. The sensor is inexpensive, easy to manufacture and fast and it is potentially useful for AD-related biomarker screening after further validation.

Keywords: Functionalized liquid crystal microcavity, Whispering Gallery Mode, Alzheimer's disease markers, biosensing platform

1. Introduction

Alzheimer's disease (AD) is a progressive and fatal neurodegenerative disorder. It is primarily characterized by progressive impairment in memory, language, cognition, and executive function, often accompanied by neurological symptoms. This condition places a significant burden on both families and society [1]. Compelling evidences indicate that the aggregation and neurotoxicity of β-amyloid (Aβ) protein are the primary causes of AD [2]. Amyloid precursor protein (APP) is initially cleaved by β-secretase to generate Aβ. Aβ aggregate into oligomers and their decreased solubility promotes deposition into plaques. Subsequently, these plaques can induce the formation of neurofibrillary tangles and neuronal loss, consequently impairing the physiological functions of nerve cells [3–5]. The most common Aβ subtypes in humans are Aβ40 and Aβ42 [6]. Owing to its two additional amino acids, Aβ42 has a higher propensity for misfolding and aggregation, thereby forming plaque deposits more readily and exhibiting greater neurotoxicity [7]. Therefore, developing an accurate and highly sensitive sensing platform for the concentration of Aβ42 is of great significance for AD biomarker screening and dynamic monitoring of the disease.

The main diagnostic methods for clinical AD include monitoring of cerebrospinal fluid (CSF) markers, positron emission computed tomography (PET) and scale tests [8]. However, due to factors such as the collection of CSFs through lumbar puncture and the use of radioactive probes in PET imaging, the clinical application of these detection methods is limited. Blood testing, as the fundamental method for diagnosing various diseases, is the preferred solution to address the aforementioned problems [9]. Through the screening of blood biomarkers, unnecessary CSF/PET scans can be reduced, and the low, medium, and high risks of AD patients can be determined, ensuring that patients truly in need receive timely treatment [10]. At present, numerous studies have focused on Aβ detection in human serum, employing a range of methods, including enzyme-linked immunosorbent assay (ELISA) [1,11], fluorescence spectroscopy [12,13], electro-chemiluminescence strategy [14–16], electrochemical impedance spectroscopy [17,18]. However, these detection methods generally have some limitations, such as complex operation process, long detection cycle, expensive equipment and the need to fluorescently label the sample. Therefore, it is urgent to develop a reliable, simple, efficient and rapid method that can further realize Aβ42 signal amplification to meet the needs AD-related biomarker screening.

In recent years, liquid crystals (LCs) have gained great attention in biomarker detection due to their excellent biocompatibility, highly sensitive response and mechanical flexibility. LCs based biosensors have been widely used in many fields, such as proteins [19,20], lipids [21], vapors [22], heavy metal ions [23] and synthetic polymers [24,25]. There are also many ways to achieve Aβ42 detection based on liquid crystal biosensors. *Kemiklioglu et al.* reported a liquid crystal thin-film biosensor that can detect different concentrations of Aβ42 based on the changes in the optical signals of the sensor [26]. *Vallamkondu et al.* designed a type of liquid crystal microdroplets stabilized by surfactants and modified them with specific antibodies. When the droplets came into contact with Aβ42, the arrangement of the liquid crystal molecules were changed, enabling the early diagnosis of AD [27]. However, most LC based optical biosensors relied on visual observation or fluorescence detection to identify biomarker binding events. Naked-eye detection was prone to subjectivity and variability in perception. The limitations were further exacerbated by the sparse amount of Aβ42 in the blood, which made it challenging to capture and analyze small and critical interactions in the human body.

In this paper, a LC biosensing platform based on WGM was proposed to achieve real-time monitoring of Aβ42 concentration. The microcavity was mainly composed of 5CB molecules and DCM dye. To achieve a sensing functionality, LC microdroplets were functionalized with target-responsive aptamers to capture specific Aβ42 and reported binding events. The schematic diagram of the detection of Aβ42 concentration is shown in Fig.1. Upon target binding, the interaction between the aptamer and Aβ42 triggered the configuration change of the LC, leading to the WGM spectra shift. This change caused a decrease in the refractive index (RI), resulting in a blue shift of the spectrally resonant wavelength. It was proved that the total shift of the resonance spectrum was proportional to the Aβ42 concentration. Due to the triple amplification effect of biomolecular polarization, WGM resonance, and the orientation transition of liquid crystal molecules, the biological reaction signals at the interface were greatly enhanced, and the detection limit of Aβ42 reached 3 pg/mL. To verify its practicality, the sensor was capable of monitoring the mouse serum containing Aβ42. This multifunctional platform provides a novel strategy for Aβ42 detection and may be useful for AD-related biomarker screening after further validation.

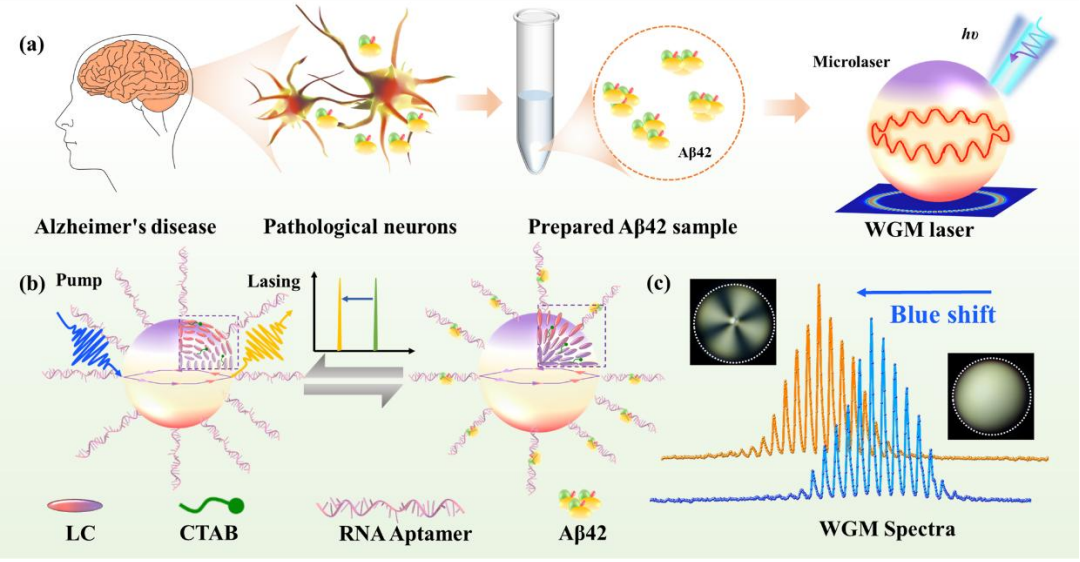

Fig. 1. Schematic concept and principle for Aβ42 concentration detection.

2 Materials and methods

2.1 Materials.

For the fabrication of LC microdroplet, the capillary was purchased from Polymicro Inc. The LC microdroplets were composed of 4-dicyano-methylene-2-methyl-6-(4-dimethylaminostyryl)−4H-pyan (DCM, 95%, Aladdin) and 4-cyano-4'-n-pentyl-1,1'-biphenyl (5CB, 98%, Aladdin). The LC microdroplet was functionalized modified using hexadecyl trimethyl ammonium bromide (CTAB, Aladdin) and RNA aptamer. The Aβ42 recognition element used in this study was derived from the RNA aptamer sequence reported by Murakami et al. [28]. The sequence was 5'-GGG ACG AAG ACC AAC UGA ACU UUU GGG UGG UAA CAG GUA GCU CCG GUU GUC CUU UGU CCG UGC UGC CAC CUU ACU UC-3' (Hongxun Biotechnology Co., LTD). Amyloid β Peptide (1-42), Amyloid β Peptide (1-40), Tau protein and a-Synuclein were purchased from Beyotime Biotechnology Co., LTD. Albumin (Aladdin), and adrenaline (Aladdin) were selected to verify the specific recognition ability of the sensor. Calcium chloride, magnesium chloride, iron chloride, glutathione and ascorbic acid were purchased from Aladdin. The test solutions were prepared using phosphate-buffered saline (PBS, Aladdin).

2.2 Preparation of Aβ42 and RNA aptamer solutions

Freeze-dried RNA aptamer should be stored under low-temperature and dry conditions. Before use, prepare it as a reserve solution with PBS solution, and store it in aliquots at −20°C to avoid repeated freezing and thawing. Before use, the RNA

aptamer was renatured on ice at room temperature. The RNA aptamer was then diluted with PBS to the desired concentration and used immediately for CTAB/aptamer functionalization and Aβ42 detection to minimize the effects of RNA degradation.

Aβ42 peptide was handled carefully because it is prone to aggregation. The lyophilized Aβ42 peptide was equilibrated to room temperature and then dissolved in 2 mM NaOH to prepare a stock solution at a concentration of 1 mg/mL. The solution was subjected to ultrasonic treatment for 5 mins to facilitate dissolution. The stock solution was aliquoted and stored at −20°C to avoid repeated freeze–thaw [29,30]. Before each experiment, one aliquot was thawed on ice and immediately diluted with PBS or serum matrix to the desired working concentrations. The freshly prepared working solutions were used for subsequent sensing experiments.

The RNA aptamer solution was prepared in PBS solution. For target recognition, equal volumes of CTAB solution and RNA aptamer solution were mixed and pre-incubated at 25°C for 20 mins to promote the formation of the CTAB–aptamer complex. Subsequently, different concentrations of Aβ42 solution were added for LC-WGM spectral detection.

2.3 Preparation of LC biosensors.

LC biosensor was prepared by conical capillary pumping method. The self-made microtubule with a diameter of 5 μm was prepared. One end of the self-made microtubule was connected to the microchannel controlled by the pump. By controlling the pumping state, 5CB microdroplets of the required size were generated in the water environment. To excite the WGM laser, 0.1 wt% DCM dye was doped into 5CB ultrasonically mixed for 20 mins and under dark conditions for storage. 5CB serves as the sensing core because of its stable nematic phase at room temperature and highly sensitive response to interfacial anchoring changes. DCM acts as the optical gain medium, generating fluorescence emission and enabling WGM lasing under 532 nm laser pumping. It should also be noted that the LC microdroplets in the experiment were generated and controlled by self-made microtubules, and only one microdroplet could be produced at a time. Each experiment was repeated at least three times to minimize false positive results and to avoid artifacts.

2.4 Optical measurement.

A typical microsystem was used to excite and collect the WGM spectra from the microdroplet. The 532 nm Nd:YAG pulse laser was used to realize optical pumping. All

WGM emission spectra were collected by a high-resolution spectrometer. All images were obtained using a charge-coupled device (CCD) camera. Polarizing optical microscope (POM, Olympus) observed LC microdroplet image.

2.5 Functionalized LC microcavities characterization.

In this study, the detection of the Aβ42 peptide is involved to monitor the structural transition of LC microdroplets, and the concentrations of CTAB and the RNA aptamer must be optimized for accurate sensing. Initially, the 5CB microdroplets were immersed in the CTAB solution to determine the concentration of CTAB. The experimental results are shown in Fig.2(a). CTAB molecules were induced to spontaneously adsorb on the surface of microdroplets. This triggered a self-assembly transition at the water/LC interface due to amphiphilicity [31]. With increase of CTAB concentration, LC microdroplet transformed into radial structures, and the structural transformation was completed at the concentration of 1 μM. After that, the RNA aptamer was injected into the solution to adsorb CTAB molecules. Because of the electrostatic interaction, CTAB formed a complex with the negatively charged RNA aptamer, which effectively separates these molecules from the droplet surface and causes the LC microdroplet to change from a radial configuration to a bipolar configuration. The final configuration of LC microdroplet depended on the concentration of aptamers. When the concentration of CTAB is 1 μM, the limiting aptamer concentration was 3 μM. As the concentration of aptamers increases from 0 to 3 μM, significant changes were observed in POM images. The cross-shaped pattern characteristic gradually disappeared and transformed into circular spots characteristic, as displayed in Fig.2(b).

Fig.2(c) shows the WGM spectrum of LC microcavities modified with CTAB and RNA aptamer. The experimental setup was shown in Fig.S1. The microcavity has an almost perfect spherical geometric shape and a smooth surface, which facilitates the interaction between light and matter, thereby promoting WGM generation. The gain medium within the microcavity was excited by free-space coupling and the photoluminescence spectrum were collected from the leakage mode and non-directional emission emitted from the non-resonant region. For the microsphere with a diameter of 80 μm (Fig.S2), the broad spontaneous emission peaked at approximately 625 nm. As the pump fluence increased, distinct lasing spikes appeared at regular intervals, and the photoluminescence (PL) intensity increased significantly. The clear threshold behavior observed in these plots confirmed that the microsensors were

exhibiting lasing action. The bright ring boundary of the DCM-5CB microsphere indicated the formation of a typical WGM resonant microcavity, as shown in Fig.S3. The measured lasing spectrum corresponded to the first-order TE modes from 551 to 563, consistent with the theoretical calculations (Equation (S1)).

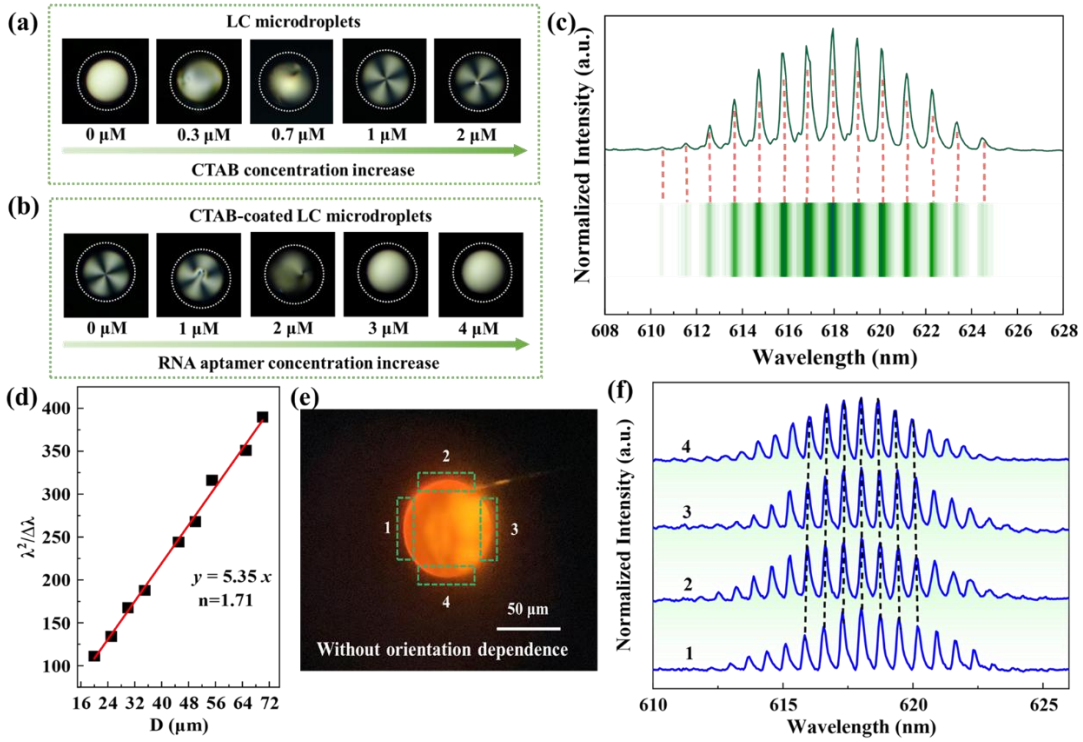

Fig. 2. (a) LC microcavity conformation under different concentration of CTAB. (b) LC microcavity conformation under different concentration of CTAB and RNA aptamer. (c)Typical WGM laser spectra. (d) Relationship between $\lambda^2/\Delta\lambda$ and the diameter of functionalized LC microcavities. (e) PL images of the functionalized LC microcavities. Rectangles 1-4 showed the regions for micro-area PL measurements. Scale bar was 50 μm. (f) Spectra recorded from four different positions within the regions marked in (e).

Considering that the size of the microsensor has a significant impact on the modulated spectrum, the relationship between the size of the microsensor and the WGM resonance has demonstrated. As shown in Fig. S4, with the diameter of LC microsensor increased from 45 μm to70 μm, the mode spacing between adjacent peaks decreased from 1.66 nm to 0.99 nm. According to WGM theory, the mode interval ($\Delta\lambda$) and diameter (D) of a microsensor were related by the equation $\lambda^2/\Delta\lambda = n\pi D$, where λ is the central emission wavelength and n is the RI. The relationship between $\lambda^2/\Delta\lambda$ and D indicated a linear fit with a slope of $n\pi$= 5.35 (Fig. 2(d)). This leaded to a RI of 1.71 [32]. Moreover, as shown in Fig. 2(d)(e), the spatially resolved WGM spectra indicated that the resonant mode remains consistent, which facilitated the identification of WGM spectra without orientation dependence.

3 Results and Discussion

In this experiment, LC microcavities with an average diameter of approximately 80 μm were generated in PBS buffer solution and systematically evaluated the effects of CTAB, RNA aptamers, and Aβ42 on the orientation of 5CB molecules within the microcavities. The experimental results were shown in Fig. 3(a). Using CTAB alone and adding Aβ42 subsequently did not cause any change in the molecular arrangement of the liquid crystal microcavities, and no morphological changes were observed in the POM images (Fig. 3(a)(I-a)-(I-f)). The results showed Aβ42 did not affect the anchoring effect of CTAB on 5CB molecules. Similarly, when the aptamer was added without CTAB, the POM image did not change either (Fig. 3(a)(I-a)-(II-a)). Even when Aβ42 was added, the structure of the liquid crystal microcavities remains unchanged (Fig. 3(a)(II-a)-(II-f)). Therefore, the presence of CTAB and aptamers is crucial for Aβ42 detection. CTAB tends to adsorb at the LC/water interface and induce radial LC orientation, whereas the negatively charged RNA aptamer electrostatically complexes with CTAB and reduces the amount of free CTAB available for interfacial anchoring, resulting in a bipolar configuration. After Aβ42 is introduced, aptamer-Aβ42 binding perturbs the aptamer–CTAB complexation equilibrium and promotes the redistribution of CTAB at the LC/water interface, thereby inducing LC director reorientation toward a radial configuration. Fig. 3(b) shows the WGM spectra corresponding to Fig. 3(a) (III-a)-(III-b). The LC microdroplets exhibited a bipolar structure and had the corresponding WGM spectrum (blue curve). When Aβ42 was added, the LC microdroplets gradually transformed from the bipolar configuration to the radial configuration (yellow curve), and showed a significant blue shift. In its initial state, the aptamer adopted a random crimp structure. When the target Aβ42 is introduced, the aptamer actually has a greater tendency to interact with Aβ42. CTAB is released, which results in LC microdroplet changes from bipolar configuration to radial configuration. For CTAB-RNA aptamer-modified 5CB microdroplets in bipolar configuration, the molecular orientation remains tangential to the spherical interface. Under these conditions, the TE mode travel along the molecules' long axis and experience the extraordinary RI (n_e=1.71). When Aβ42 is introduced, the 5CB molecules undergo reorientation from a parallel to a perpendicular alignment relative to the droplet surface. This structural transition leads to a gradual decrease in the effective dielectric constant

($n_o \leq n \leq n_e$), thereby causing a blue shift in the WGM spectrum, as shown in Fig. 3(c)(d) (Equation (S2)). The electric field distribution within the LC microcavity was analyzed, as shown in Fig. 3(e). Furthermore, Fig. 3(f) showed the changes in free spectral range (FSR) within the five independent LC microcavity conducted below. It has been proved that the microcavity has good stability and reproducibility, and is suitable for subsequent detection of Aβ42 concentration.

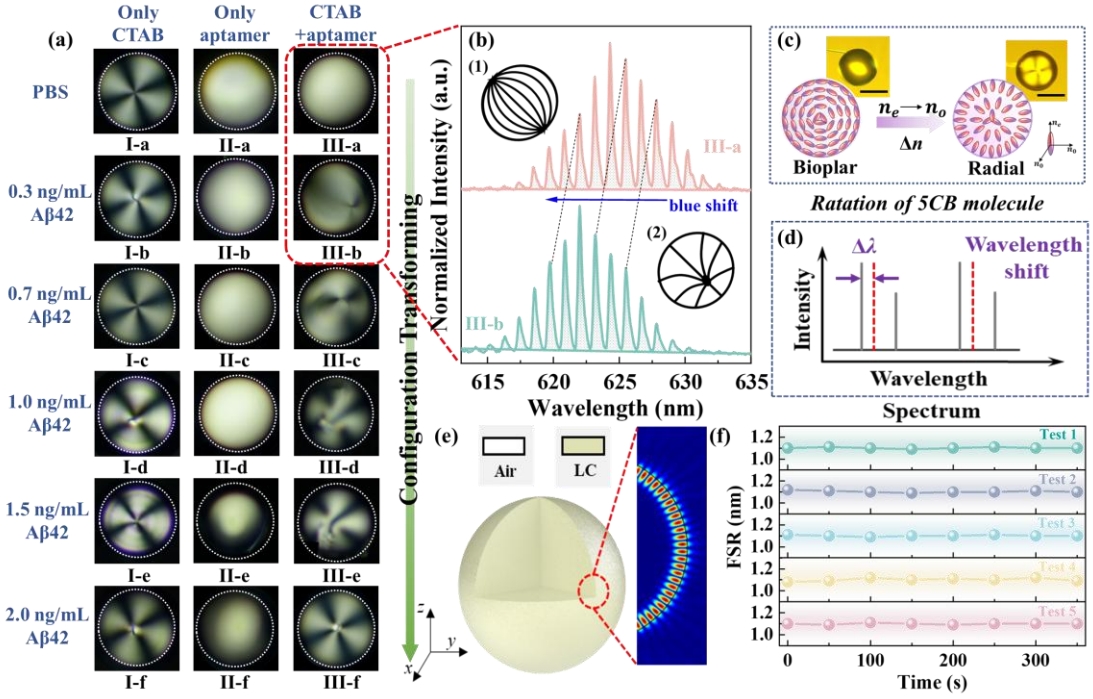

Fig. 3 (a) POM images of LC microdroplets in different solution environment (I, only CTAB; II, only aptamer; III, CTAB + aptamer). (b) WGM spectra a of functionalized-LC microcavity under different Aβ42 concentration. Inset (1) and (2) shows bipolar and radial configurations, respectively. (c)(d) Different orientations of the 5CB molecules, as well as the corresponding POM images and LC microdroplets diagrams. (e) Simulated structure of LC microcavity and the radial electric field distribution within the structure. (f) Variation of FSR in different LC microcavities.

Based on the above sensing mechanism, the sensing performance under different concentrations of Aβ42 was evaluated. Fig. 4(a)(b) showed the observed spectral response and the sensitivity of the sensing platform at different Aβ42 concentrations. The concentration of Aβ42 has a linear relationship with the WGM wavelength shift. The sensor demonstrated a sensitivity of approximately 0.003 nm/pg/mL and an excellent linear correlation (R^2= 99.8%). Based on the formula Limit of detection (LOD)= 3σ/slope, where σ is the standard deviation, and slope is the sensitivity of the sensor. The LOD of the sensor is as low as 3 pg/mL. At a concentration of 250 pg/mL for Aβ42, although the POM image did not show obvious changes, the WGM spectrum showed a significant wavelength variation, which once again proved that the sensitivity of the WGM barcode was much higher than that of the POM method, as displayed in

Fig. 4(c)(d). The response times were also systematically recorded across a range of Aβ42 concentrations, as illustrated in Fig. 4(e)(f). As the concentration of Aβ42 increases, the reaction time accelerates. It is worth noting that the peak intensity of WGM remained basically stable throughout the detection period (Fig. 4(g)). Furthermore, the environmental temperature plays a crucial role in the field of liquid crystal microcavity biosensing (Fig. S8). Fig. 4(h) shows the WGM spectrum at concentration of 250 pg/mL Aβ42.

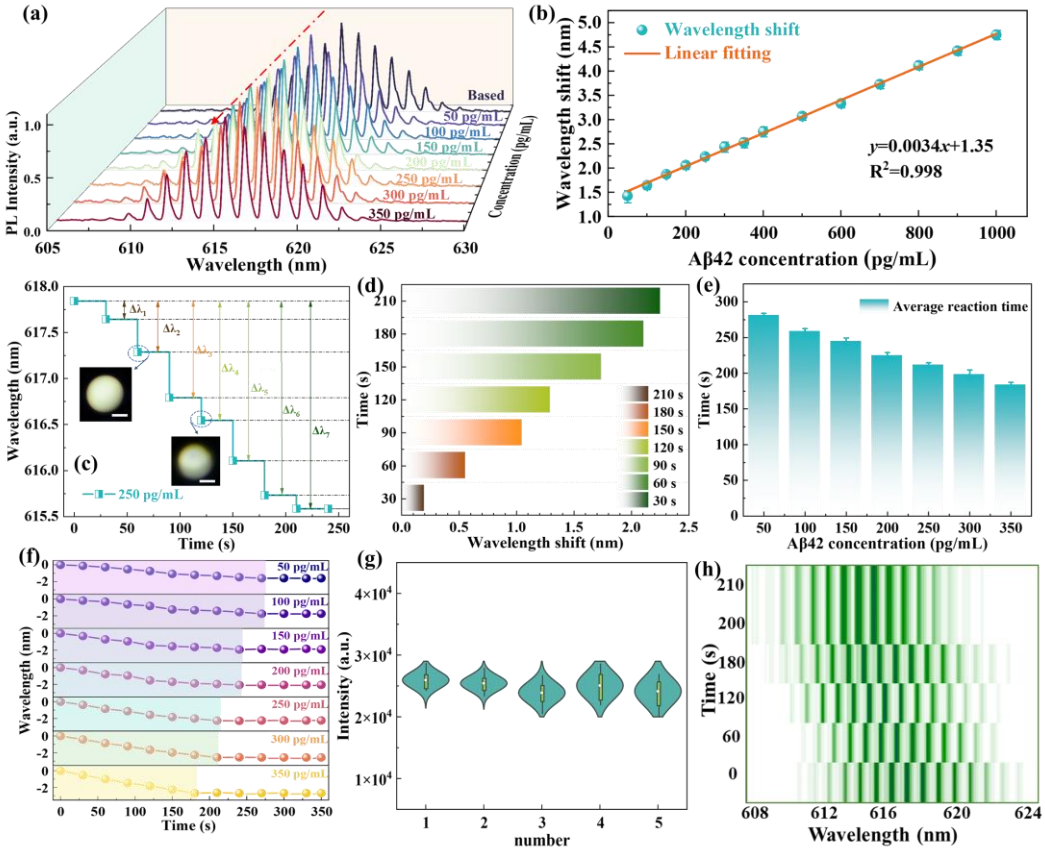

Fig. 4 (a) The WGM spectrum response of the LC biosensor at different Aβ42 concentrations. The blueshift of the wavelength occurred with the increasing Aβ42 concentration. (b) The linear fitting for determining the sensitivity of Aβ42 detection. (c) WGM-resonant wavelength for reaction time during 250 pg/mL Aβ42. (d) The wavelength shifts of resonance peak, relative to the initial time point. (e) The linear fitting of Aβ42 concentration with reaction time. (f) Temporal dependence of WGM wavelength shift with different Aβ42 concentrations. (g) Intensity of WGM peaks during detection period. (h) The WGM spectra response of the LC biosensor recorded at different time intervals following the addition of 250 pg/mL Aβ42.

Specificity is among the most important characteristics for biosensors. To evaluate the specific recognition of the Aβ42 biosensor, the other common serum interfering substances, such as Aβ40, tau protein or α-synuclein were introduced. A controlled experiment with a solution of 0 ng/mL Aβ42 was performed, which produced either a negligible or no spectral response. As shown in Fig. 5(a)(b), the WGM spectra and POM

images of the biosensor were presented after adding the mixture of (a) PBS, aptamers, and CTAB, (b) 1000 pg/mL Aβ40, aptamers, and CTAB, (c) 1000 pg/mL tau protein, aptamers, and CTAB; (d) 1000 pg/mL α-synuclein, aptamers, and CTAB. Compared with the wavelength shift caused by Aβ42, in the cases where only Aβ40, tau protein or α-synuclein interfering protein was present, the biosensor failed to produce significant spectral responses and POM changes. This verified the high specificity of the sensor for Aβ42 recognition.

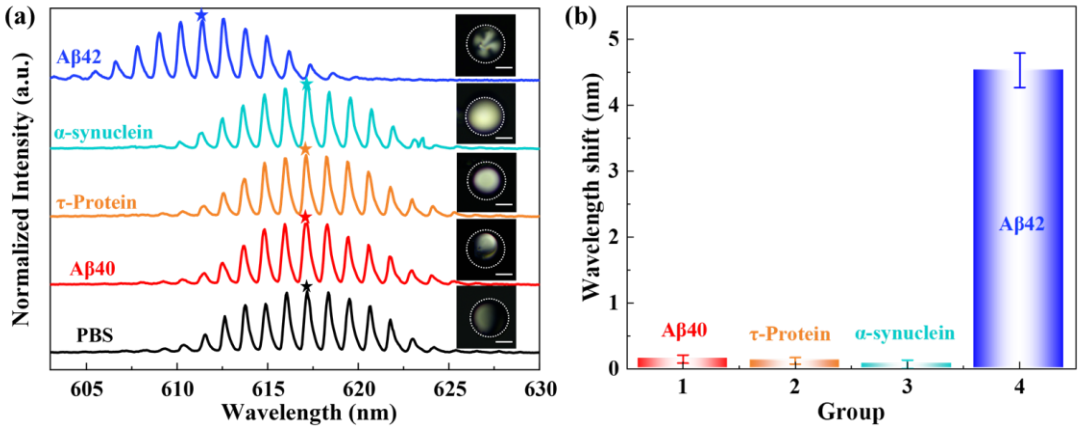

Fig.5 The specificity test of the Aβ42 sensing. (a) The WGM spectrum response of PBS, Aβ40, tau protein, α-synuclein, and 1000 pg/mL Aβ42. (b) The wavelength shift of the WGM spectrum and the positive number represents blueshift.

To demonstrate the specificity of the sensing element itself, a non-aptamer sequence of the same length as a control. The experimental results are shown in Fig. S5. When 1 ng/mL Aβ42 was introduced, the group with a non-aptamer sequence did not cause any conformational change in the LC microdroplet. At this time, the LC microdroplet still maintained a bipolar configuration. In other words, it indicates that only the RNA aptamer in the experiment can specifically recognize Aβ42. Meanwhile, to simulate the human environment, complex substances such as adrenaline and human serum albumin to investigate were introduced to the sensor. The experimental results are shown in Fig. S6. Due to the lack of specific binding between saline/ adrenaline/ albumin, and aptamers, the interference solution did not cause significant wavelength shift. A slight red shift was observed, possibly caused by increased RI. However, this effect was almost negligible when compared to the significant blue shift observed with Aβ42. Additional interference tests were performed using Na^+, K^+, Ca^{2+}, Mg^{2+}, Fe^{3+}, glutathione, and ascorbic acid, as shown in Fig. S7. PBS containing Na^+, K^+, and phosphate ions showed negligible background response. These interferents caused no obvious POM change. These significant differences highlighted the strong specificity

and reliability of LC biosensor for Aβ42 detection, even in complex environments.

To evaluate the potential of LC biosensor for the detection of Aβ42 concentrations in serum samples, healthy mouse serum without dilution was used for the assay to evaluate the feasibility of the biosensor in a challenging serum matrix. While CTAB and RNA concentrations were maintained at 1 μM and 3 μM, respectively. The concentration of Aβ42 in the serum of normal people is 50 pg/mL, while the serum-Aβ42 concentration of patients with AD is lower than that of normal people. So the testing Aβ42 concentration was prepared in the range from 0 pg/mL-50 pg/mL. In this instance, the serum was employed as the aqueous environment.

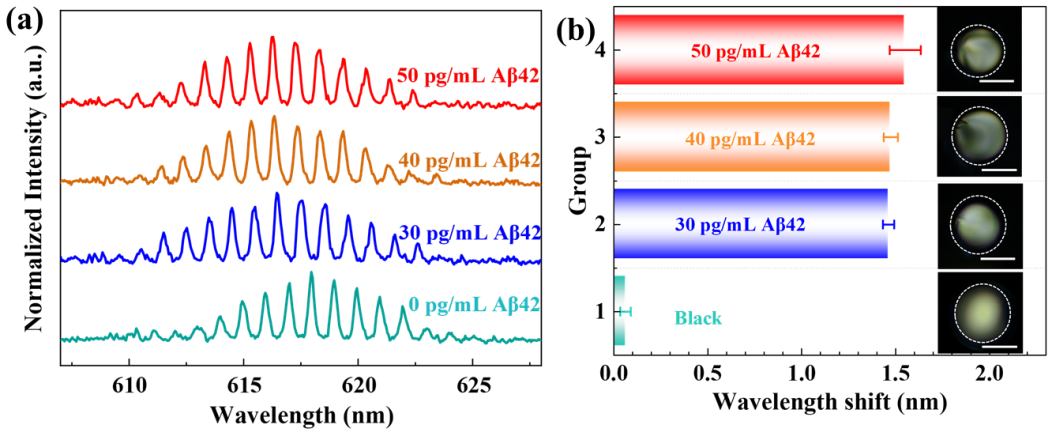

Fig.6 (a) WGM spectral response under different Aβ42 concentrations. (b) WGM wavelength shift during Aβ42 concentration increases from 0 pg/mL to 50 pg/mL. Inset images shows the corresponding POM images.

Fig. 6(a) showed the WGM spectra and corresponding POM images from the sensor after adding a mixture of Aβ42 in serum with different concentrations, aptamers, and CTAB. It was illustrated that distinguishing morphological differences in POM images for varying Aβ42 concentrations posed a challenge. In contrast, the WGM spectra clearly exhibited a distinct blueshift. As shown in Fig.6(b), a positive correlation was observed between the wavelength shift and Aβ42 concentration. By measuring this wavelength shift, The Aβ42 concentrations were calculated according to the sensitivity profile shown in Fig.4(b). The measured Aβ42 concentrations in serum sample were 32, 36, and 40.8 pg/mL, respectively. Consequently, the recovery ratios obtained from three spiked serum samples, tested with Aβ42 concentrations ranging from 30 to 50 pg/mL, were 106%, 90%, and 81.6%, respectively. Some possible reasons for this include: Matrix effects, nonspecific adsorption, and background RI variations in serum may cause both positive and negative deviations [8,33,34]. In future work, the serum pretreatment procedure and matrix-matched calibration method will be optimized to

reduce nonspecific adsorption, thereby improving the recovery and reproducibility of Aβ42 detection in serum. In addition, serum samples from different sources will be used to further validate the practical performance of the biosensing platform.

In this study, LC biosensing platform was developed for the determination of Aβ42 concentration. As demonstrated in Table S1, the LC microcavity that was prepared featured a simple structure, and the detection performance of LCs in the serum sample was also studied with satisfactory results. The detection limit was 3 pg/mL. Compared with the POM method, the biological reaction is transformed from the LC biosensor into resonance spectroscopy. This change makes it possible to analyze the reaction process quantitatively, to detect low concentrations and to identify subtle changes. Compared with ELISA and electrochemical sensors, this sensor does not require labeling and has strong specificity in recognition. The WGM resonance response is significantly enhanced due to the synergistic effects of light-matter interaction and the change in LC orientation, which are triggered by the target information. And aptamers were used as functional modifications to improve the sensor's specific recognition ability[15,35]. In the future, the LC biosensor with deep learning for AD detection in human serum samples, which would be a good choice for clinical trials[35].

5 Conclusion

In this study, an aptamer-LC based biosensor was used to establish detect Aβ42 concentration in serum sample. The new approach leveraged strong light-matter interactions within LC-WGM microcavity, providing opportunities for sensing and amplifying subtle target-binding events. The ability of the sensor was demonstrated by the detection of Aβ42 using the LC microcavity. The shift of WGM spectra was used as an indicator to confirm to binding Aβ42 content detected by the LC microcavity. The results highlighted the role of LC microcavity as a highly sensitive and selective platform for detecting and amplifying specific Aβ42 binding events. Additionally, the functional versatility of aptamer-modified LC microcavities allowed direct adaptation to detect a diverse array of targets, encompassing both nucleic acids and small-molecule compounds. At the same time, the compact size of LC microdroplets also offers possibilities for wearable applications. It can be envisioned that this platform is potentially useful for Aβ42 monitoring and may contribute to future AD-related biomarker screening after validation in human serum and clinical cohorts.

Authors Contributions

Peiyao An: Writing – review & editing, Writing – original draft, Conceptualization, Methodology. Mengxiao Li: Writing – original draft, Data curation, Investigation. Shanshan Zhang: Writing review, Formal analysis. Di Lian: Investigation, Supervision. Chuqi Li: Methodology. Chuan Wang: Methodology. Miao Yu: investigation. Duo Wang: Methodology. Lingyi Kong: Formal analysis. Jun Ren: Methodology, Conceptualization, Supervision. Yue Li: Methodology. Haiyan Wang: Supervision. Xin Yang: Supervision. Zhenlin Wu: Methodology, Resources, Validation, Supervision and Project Administration. All authors contributed to the general discussion.

Declaration of competing interest

There are no conflicts to declare.

Acknowledgements

This work was funded by project "Fundamental Research Funds for the Central Universities (DUT25YG256)".

Data availability

Data will be made available on request.

References

[1] M. Sardar Sinha, A. Ansell-Schultz, L. Civitelli, C. Hildesjö, M. Larsson, L. Lannfelt, M. Ingelsson, M. Hallbeck, Alzheimer's disease pathology propagation by exosomes containing toxic amyloid-beta oligomers, Acta Neuropathol 136 (2018) 41–56. https://doi.org/10.1007/s00401-018-1868-1.

[2] O.E. Eremina, N.R. Yarenkov, G.I. Bikbaeva, O.O. Kapitanova, M.V. Samodelova, T.N. Shekhovtsova, I.E. Kolesnikov, A.V. Syuy, A.V. Arsenin, V.S. Volkov, G.I. Tselikov, S.M. Novikov, A.A. Manshina, I.A. Veselova, Silver nanoparticle-based SERS sensors for sensitive detection of amyloid-β aggregates in biological fluids, Talanta 266 (2024) 124970. https://doi.org/10.1016/j.talanta.2023.124970.

[3] M.A. Findeis, The role of amyloid β peptide 42 in Alzheimer's disease, Pharmacology & Therapeutics 116 (2007) 266–286. https://doi.org/10.1016/j.pharmthera.2007.06.006.

[4] R.G. Canter, J. Penney, L.-H. Tsai, The road to restoring neural circuits for the treatment of Alzheimer's disease, Nature 539 (2016) 187–196. https://doi.org/10.1038/nature20412.

[5] H.T. Ngoc Le, J. Park, S.R. Chinnadayyala, S. Cho, Sensitive electrochemical detection of amyloid beta peptide in human serum using an interdigitated chain-shaped electrode, Biosensors and Bioelectronics 144 (2019) 111694. https://doi.org/10.1016/j.bios.2019.111694.

[6] X. Li, M. Yuan, T. Han, Q. Han, L. Yao, X. Song, A novel photoelectrochemical aptasensor for Aβ42 monomer detection based on in-situ grown covalent organic frameworks, Microchemical Journal 217 (2025) 114974. https://doi.org/10.1016/j.microc.2025.114974.

[7] K. Luo, B. Zhang, Y. Mei, S. Rong, K. Wang, P. Liu, Q. Yao, B. He, B. Hao, P. Cheng, T. Jiang, Q. Hu, A piezoelectric enhanced and self-calibrating SERS platform based on Ag nanocubes-modified polyvinylidene fluoride for ultrasensitive and simultaneous detection of Aβ40 and Aβ42, Sens. Actuators, B 446 (2026) 138685. https://doi.org/10.1016/j.snb.2025.138685.

[8] D. Böken, Z. Xia, J.Y.L. Lam, E. Fertan, Y. Wu, E.A. English, J. Konc, F. Layburn, G.J.L. Bernardes, H. Zetterberg, M.R. Cheetham, D. Klenerman, Ultrasensitive Protein Aggregate Quantification Assays for Neurodegenerative Diseases on the Simoa Platform, Anal. Chem. 97 (2025) 290–299. https://doi.org/10.1021/acs.analchem.4c04188.

[9] B.S. Rauchmann, T. Schneider-Axmann, R. Perneczky, Associations of longitudinal plasma p-tau181 and NfL with tau-PET, aβ-PET and cognition, J. Neurol. Neurosurg. Psychiatry 92 (2021) 1289–1295. https://doi.org/10.1136/jnnp-2020-325537.

[10] A. Nakamura, N. Kaneko, V.L. Villemagne, T. Kato, J. Doecke, V. Doré, C. Fowler, Q.-X. Li, R. Martins, C. Rowe, T. Tomita, K. Matsuzaki, K. Ishii, K. Ishii, Y. Arahata, S. Iwamoto, K. Ito, K. Tanaka, C.L. Masters, K. Yanagisawa, High performance plasma amyloid-β biomarkers for alzheimer's disease, Nature 554 (2018) 249–254. https://doi.org/10.1038/nature25456.

[11] C. Peng, R.J. Gathagan, D.J. Covell, C. Medellin, A. Stieber, J.L. Robinson, B. Zhang, R.M. Pitkin, M.F. Olufemi, K.C. Luk, J.Q. Trojanowski, V.M.-Y. Lee, Cellular milieu imparts distinct pathological α-synuclein strains in α-synucleinopathies, Nature 557 (2018) 558–563. https://doi.org/10.1038/s41586-018-0104-4.

[12] A.G. Karkisaval, R. Hassan, A. Nguyen, B. Balster, F. Abedin, R. Lal, S.A. Tatulian, The structure of tyrosine-10 favors ionic conductance of Alzheimer's disease-associated full-length amyloid-β channels, Nat Commun 15 (2024). https://doi.org/10.1038/s41467-023-43821-y.

[13] N. Trinh, K.R. Bhuskute, N.R. Varghese, J.A. Buchanan, Y. Xu, F.M. McCutcheon, R.L. Medcalf, K.A. Jolliffe, M. Sunde, E.J. New, A. Kaur, A Coumarin-Based Array for the Discrimination of Amyloids, ACS Sens. 9 (2024) 615–621. https://doi.org/10.1021/acssensors.3c01334.

[14] H. Ke, H. Sha, Y. Wang, W. Guo, X. Zhang, Z. Wang, C. Huang, N. Jia, Electrochemiluminescence resonance energy transfer system between GNRs and Ru(bpy)32+: Application in magnetic aptasensor for β-amyloid, Biosensors and Bioelectronics 100 (2018) 266–273. https://doi.org/10.1016/j.bios.2017.09.017.

[15] J.-X. Wang, Y. Zhuo, Y. Zhou, H.-J. Wang, R. Yuan, Y.-Q. Chai, Ceria Doped Zinc Oxide Nanoflowers Enhanced Luminol-Based Electrochemiluminescence Immunosensor for Amyloid-β Detection, ACS Appl. Mater. Interfaces 8 (2016) 12968–12975. https://doi.org/10.1021/acsami.6b00021.

[16] N.G. Margraf, U. Jensen-Kondering, C. Weiler, F. Leypoldt, W. Maetzler, S. Philippen, T. Bartsch, C. Flüh, C. Röcken, B. Möller, G. Royl, A. Neumann, N. Brüggemann, B. Roeben,

C. Schulte, B. Bender, D. Berg, G. Kuhlenbäumer, Cerebrospinal Fluid Biomarkers in Cerebral Amyloid Angiopathy: New Data and Quantitative Meta-Analysis, Front. Aging Neurosci. 14 (2022). https://doi.org/10.3389/fnagi.2022.783996.

[17] C. Robinson, V.B. Juska, A. O'Riordan, Surface chemistry applications and development of immunosensors using electrochemical impedance spectroscopy: A comprehensive review, Environmental Research 237 (2023) 116877. https://doi.org/10.1016/j.envres.2023.116877.

[18] J. Qin, J.S. Park, D.G. Jo, M. Cho, Y. Lee, Curcumin-based electrochemical sensor of amyloid-β oligomer for the early detection of Alzheimer's disease, Sensors and Actuators B: Chemical 273 (2018) 1593–1599. https://doi.org/10.1016/j.snb.2018.07.078.

[19] H.K. Bisoyi, Q. Li, Liquid crystals: Versatile self-organized smart soft materials, Chem. Rev. 122 (2022) 4887–4926. https://doi.org/10.1021/acs.chemrev.1c00761.

[20] H. Maheshwari, P.M. Naveenkumar, R.K. Singh, L. Soni, K.P. Sharma, Charge modulation at the liquid crystal droplet-aqueous interface enables ultrasensitive, nonspecific protein detection, Small 20 (2024) 2407077. https://doi.org/10.1002/smll.202407077.

[21] P. Bao, K. Phillips, R. Raval, Membrane proteins in action monitored by pH-responsive liquid crystal biosensors, ACS Appl. Mater. Interfaces 16 (2024) 31843–31850. https://doi.org/10.1021/acsami.4c06614.

[22] Z. Chen, S. Fu, Y. Guan, High-sensitive liquid crystal-based optical sensor for real-time detection of formaldehyde vapor, Sensors and Actuators B: Chemical 431 (2025) 137424. https://doi.org/10.1016/j.snb.2025.137424.

[23] A. Verdian, Z. Khoshbin, C.-H. Chen, Q. Hu, Attomolar analyte sensing technique for detection of Pb2+ and Hg2+ ions based on liquid crystal, Talanta 253 (2023) 124042. https://doi.org/10.1016/j.talanta.2022.124042.

[24] Z. Khoshbin, A. Verdian, S.M. Taghdisi, N.M. Danesh, K. Abnous, A novel liquid crystal assay based on aptazyme-assisted bioprobe for ultra-sensitive monitoring of lead ion, Sens. Actuators, B 375 (2023) 132926. https://doi.org/10.1016/j.snb.2022.132926.

[25] P. An, M. Li, S. Zhang, Z. Cao, M. Yu, T. Huang, D. Wang, Y. Li, R. Shen, X. Yang, J. Ren, Z. Wu, Liquid crystal biosensor with aptamer recognition for highly sensitive and quantitative norfloxacin detection via whispering gallery mode, Microchemical Journal 221 (2026) 116766. https://doi.org/10.1016/j.microc.2025.116766.

[26] E. Kemiklioglu, E.B. Tuncgovde, G. Ozsarlak-Sozer, Development of liquid crystal biosensor for the detection of amyloid beta-42 levels associated with alzheimer's disease, J. Biosci. Bioeng. 132 (2021) 88–94. https://doi.org/10.1016/j.jbiosc.2021.03.016.

[27] S.R. Pradhan, R.S. Pathinti, R. Kandimalla, K. Chithari, M.R. Veeramalla N., J. Vallamkondu, Label-free detection of aβ-42: A liquid crystal droplet approach for alzheimer's disease diagnosis, RSC Adv. 14 (2024) 12107–12118. https://doi.org/10.1039/D4RA00615A.

[28] K. Murakami, Y. Obata, A. Sekikawa, H. Ueda, N. Izuo, T. Awano, K. Takabe, T. Shimizu, K. Irie, An RNA aptamer with potent affinity for a toxic dimer of amyloid β42 has potential utility for histochemical studies of alzheimer's disease, J. Biol. Chem. 295 (2020) 4871–4880. https://doi.org/10.1074/jbc.RA119.010955.

[29] H. Sohrabnavi, M. Mohammadimasoudi, H. Hajghassem, Early detection of Alzheimer's disease by measuring amyloid beta-42 concentration in human serum based on liquid crystals, Sensors and Actuators B: Chemical 401 (2024) 134966. https://doi.org/10.1016/j.snb.2023.134966.

[30] E. Kemiklioglu, E.B. Tuncgovde, G. Ozsarlak-Sozer, Development of liquid crystal biosensor for the detection of amyloid beta-42 levels associated with alzheimer's disease, Journal of Bioscience and Bioengineering 132 (2021) 88–94. https://doi.org/10.1016/j.jbiosc.2021.03.016.

[31] D.S. Miller, X. Wang, N.L. Abbott, Design of Functional Materials Based on Liquid Crystalline Droplets, Chem. Mater. 26 (2014) 496–506. https://doi.org/10.1021/cm4025028.

[32] B. Xu, S. Yang, X. Feng, T. Zhang, Z. Gao, Y.S. Zhao, Dual-stimuli responsive photonic barcodes based on perovskite quantum dots encapsulated in whispering-gallery-mode microspheres, Journal of Materiomics 9 (2023) 423–430. https://doi.org/10.1016/j.jmat.2022.12.009.

[33] X. Zhan, Y. Liu, K.-L. Yang, D. Luo, State-of-the-art development in liquid crystal biochemical sensors, Biosensors 12 (2022) 577–614. https://doi.org/10.3390/bios12080577.

[34] X. Wang, Y. Zhu, T.R. Olsen, N. Sun, W. Zhang, R. Pei, Q. Lin, A graphene aptasensor for biomarker detection in human serum, Electrochim. Acta 290 (2018) 356–363. https://doi.org/10.1016/j.electacta.2018.08.062.

[35] L. Liu, N. Xia, J. Zhang, W. Mao, Y. Wu, X. Ge, A graphene oxide-based fluorescent platform for selective detection of amyloid-β oligomers, Anal. Methods 7 (2015) 8727–8732. https://doi.org/10.1039/c5ay02018b.